Chinese Chemical Letters 33 (2022) 497–500

Contents lists available at ScienceDirect

Chinese Chemical Letters

journal homepage: www.elsevier.com/locate/cclet

Automated and remote synthesis of poly(ethylene glycol)-mineralized ZIF-8 composite particles *via* a synthesizer assisted by femtosecond laser micromachining

Miao Wu[a,b,c], Lingling Xia[a], Yucen Li[a], Difeng Yin[d,e], Jianping Yu[d,e], Wenbo Li[d,e], Ning Wang[f], Xin Li[a], Jiwei Cui[f,*], Wei Chu[a,c,*], Ya Cheng[a,b,c,d,e,*], Ming Hu[a,*]

[a] *School of Physics and Electronic Science, East China Normal University, Shanghai 200241, China*
[b] *State Key Laboratory of Precision Spectroscopy, School of Physics and Electronic Science, East China Normal University, Shanghai 200241 China*
[c] *XXL – The Extreme Optoelectromechanics Laboratory, School of Physics and Electronic Science, East China Normal University, Shanghai 200241 China*
[d] *State Key Laboratory of High Field Laser Physics and CAS Center for Excellence in Ultra-intense Laser Science, Shanghai Institute of Optics and Fine Mechanics (SIOM), Chinese Academy of Sciences (CAS), Shanghai 201800, China*
[e] *University of Chinese Academy of Sciences, Beijing 100049, China*
[f] *Key Laboratory of Colloid and Interface Chemistry of the Ministry of Education, School of Chemistry and Chemical Engineering, Shandong University, Ji'nan 250100, China*

ARTICLE INFO

Article history:
Received 24 May 2021
Revised 15 June 2021
Accepted 2 July 2021
Available online 8 July 2021

Keywords:
ZIF-8
Automatic synthesis
Remote synthesis
MOFs
Vaccine particles
Microfluidic chip
Flow chemistry

ABSTRACT

Mineralization of the ZIF-8 in the presence of biomacromolecules has been demonstrated to be a general way for making bioentities@ZIFs composites. The ZIF-8 crystals permit controlled storage and utilization of the bioentities, thus can benefit drug delivery, cold-chain breaking etc. With the increasing needs on personal care and distributed manufacturing, automated synthesis controlled by a computer becomes the next challenge. In this work, we designed an automatic synthesis system to prepare PEG mineralized ZIF-8 composite particles. This system is based on flow chemistry with the microfluidic chips fabricated by femtosecond laser micromachining. The particles were synthesized and monitored automatically. Furthermore, this synthesizer could be extended for fabrication of vaccine particles under remote control through internet.

Metal-organic frameworks (MOFs) are a class of solid formed by self-assembly of inorganic nodes and organic ligands [1-12]. Recently, they have been recognized as versatile matrix for encapsulating bioentities [13-18]. The MOFs work as crystalline coating for the bioentities which are useful for therapy and biocatalysis *etc.* In particular, mineralization of ZIF-8 in the presence of biomacromolecules has been demonstrated to be a general way for making the bioentities@ZIFs composites. The Zn^{2+} ions and 2-methylimidazole ligands coordinate together around the biomacromolecules, forming crystals which swallow the biomacromolecues inside. The ZIF-8 crystals permit controlled storage, release and utilization of the bioentities, thus can benefit drug delivery, cold-chain breaking *etc.* [13-18].

The formation process of the bioentities@ZIFs is naturally suitable for large-scale process. Flow chemistry has been employed for continuous synthesis of the bioentities@ZIFs. This method can enhance the reproducibility and be scaled-up easily [19,20]. With the increasing needs on personal care and distributed manufacturing, automated synthesis becomes the next challenge. Automated synthesis can monitor and regulate the synthetic process. Ideally, non-specialists will be able to obtain the target ZIF composites by simply input the aim parameter.

Recently, automated syntheses have been rapidly developed. The complex operations and parameters become controllable through algorithms such as machine learning [21]. In particular, the pharmaceutic industry is benefiting from the related technology which can certainly increase the research and development speed in a lower cost [22-28]. So far, the automated syntheses have been tried in several materials such as quantum dots, carbon nanotubes, vdW crystals, as well as metal-organic cages [29-35]. However, this technology has not been applied to mineralization of ZIF-

* Corresponding authors.
E-mail addresses: jwcui@sdu.edu.cn (J. Cui), wchu@phy.ecnu.edu.cn (W. Chu), ya.cheng@siom.ac.cn (Y. Cheng), mhu@phy.ecnu.edu.cn (M. Hu).

https://doi.org/10.1016/j.cclet.2021.07.004
1001-8417/

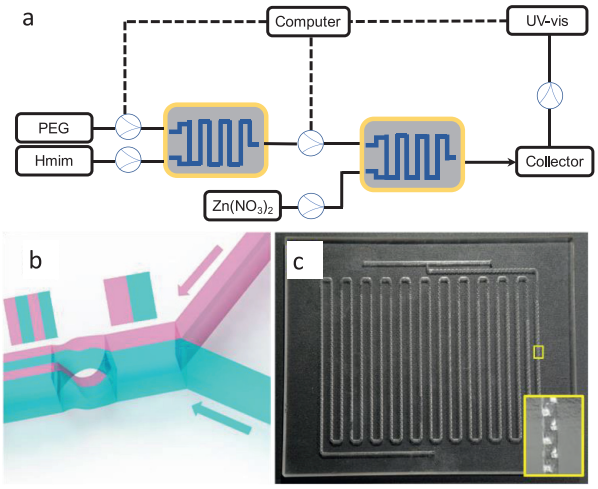

Fig. 1. (a) Illustration of the automated synthetic system. (b) Schematic view of working mechanism of the single mixing unit. (c) Photograph of the glass microfluidic chip. Inset: the close view of the mixing units at the location of the yellow box.

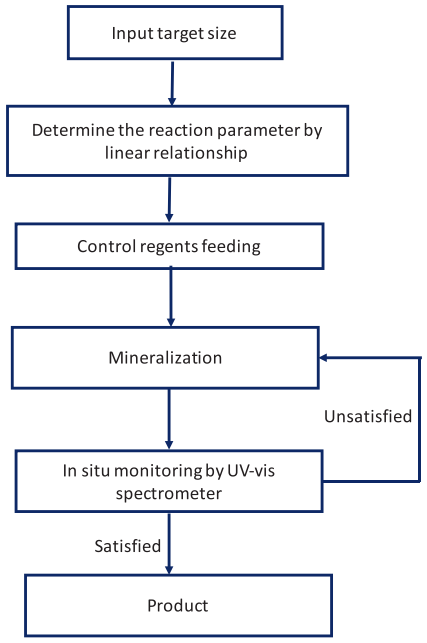

Fig. 2. A processing algorithm for automatic synthesize of PEG mineralized ZIF with controlled size.

8 composites yet. In addition, a method for in situ characterization of the products needs to be established.

In this work, we selected PEG mediated mineralization of ZIF-8 as the model reaction. This reaction allows co-encapsulation of PEG and other bioentities into the ZIF-8 crystals. The PEG mineralized ZIF-8 biocomposites have recently been proved to be useful in drug and vaccine delivery [36,37]. Automated and remote synthesis of the PEG mineralized ZIF-8 biocomposites is a step towards the future personalized synthesis of therapeutics.

The automatic mineralization of ZIF-8 particles in the presence of PEG has been realized in a synthesizer which is based on flow chemistry (Fig. S1 in Supporting information). The regents are sequentially added into the system by peristaltic pumps under the control of a computer (Fig. 1a). The reactants are mixed in our lab-made glass microfluidic chips. In brief, 2-methylimidazole and PEG (4000 MW) are mixed to a microfluidic chip first. Subsequently, the mixed solution was reacted with an aqueous solution containing $Zn(NO_3)_2$ in another microfluidic chip. The mixture was aged and monitored by UV-vis spectrometer before collected by centrifugation.

The operating principle of the mixing unit enabled by Baker's transformation is illustrated in Fig. 1b. Two different microstreams (*i.e.*, illustrated in red and green in Fig. 1b) are sent into the mixing unit, separating from each other as the right (in green) and left (in red) microstreams. After that, the two microstreams are divided into the upper and lower streams. With this manner, the number of microstreams in the microchannel can be increased from 2 to 4. Repeating of the process enables rapid increasing of the number of microstreams (N) in the main microchannel as a function of N^{2n}, where n is the number of mixing units. As a result, high mixing efficiency can be achieved by using our microfluidic chip. The chips with 3D configuration were realized in silica glass by femtosecond laser micromachining as shown in Fig. 1c. The length of each mixing unit is 2 mm, and the area of the cross-section of 1 mm × 1 mm. The chip contains 400 mixing units with a size of 110 mm × 100 mm. More details of femtosecond laser micromachining can be found in the supplementary document (Fig. S2 in Supporting information) [38-40].

The size of the product correlates to the amount of PEG molecules. Figs. S3–S6 (Supporting information) show scanning electron microscopy (SEM) images of the obtained particles. All the samples are of polyhedron shapes which are typical for ZIF-8 crystals. The statistic size distribution curves of the particles were collected by analyzing a hundred particles in each image. All the size distribution curves can be simulated as a Gaussian shape, indicating the uniform size of the samples. A relationship between the mean size and the amount of PEG has been plotted in Fig. S7 (Supporting information). The particle sizes decrease linearly with the increase of the PEG concentration. The content of PEG in the particles are approximately 25 wt% according to the thermogravimetric analysis. The role of the PEG is probably due to the interaction between the Zn^{2+} ions and the ethoxyl groups in the PEG molecules, which can stabilize the pre-nucleation clusters and prompt nucleation surrounding the molecular chains. The more the PEG molecules, the more nuclei are formed, which means that there are less Zn^{2+} and 2-methyimidazole to support growth of each nucleus. Thereby, the obtained crystals become smaller with more PEG molecules. In addition, the PEG molecules can attach on the surface of the obtained crystals, increasing the monodispersity of the particles.

For an automatic process, an *in situ* way to monitor/confirm formation the ZIF-8 is important. As a metal-organic complex, ZIF-8 has a strong ultra-violet absorption at near 200 nm. Such an absorption is probably caused by the ligand to metal charge transfer (LMCT) which correlates to the structural ZnN_4 clusters [41]. We measured UV-vis adsorption spectra of all the obtained particles. The spectra are shown in Fig. S8 (Supporting information). They all have a singlet absorption near 200 nm. This result indicates that it is possible to deduce the size of the synthesized ZIF-8 particles by an *in situ* UV-vis spectroscopy method.

For an automated synthetic system, we have strong interest to control the particle size. On the basis of a relationship shown in Fig. S7, we input the target size, and deduce the required concentration of the PEG. This parameter is used to establish an automated logarithm. A processing algorithm is designed for automatic controlling the synthesizer (Fig. 2). Basically, the target size is input into the program. The required PEG concentration is given by the linear relationship obtained from Fig. S7. Then the computer sends order to peristaltic pumps to mix reactants in microfluidic chips. After mixing, the suspension is aged for mineralization. Trace amount of the sample is taken by syringe pumps and di-

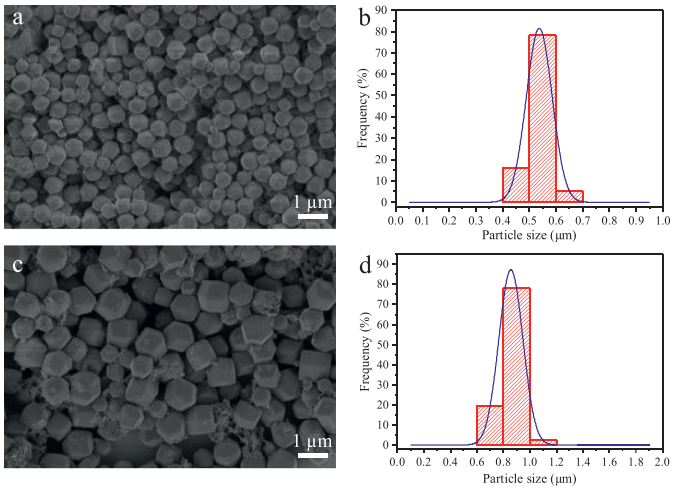

Fig. 3. (a) ZIF-8 particles synthesized automatically (particle size 500 nm). (b) Static size distribution of the particles shown in (a). (c) ZIF-8 particles synthesized automatically (particle size 900 nm). (d) Static size distribution of the particles shown in (c).

luted by distilled water. UV-vis absorption spectroscopy measures the peak near 200 nm to confirm the formation of ZIF-8. If the experimental data agrees with the calculated data, the samples are harvested as product. Otherwise, the mineralization process is continued.

We let the synthesizer to perform syntheses automatically (Fig. S9 in Supporting information). Fig. 3 illustrates SEM images of the as-prepared samples. The particles were further characterized by powder X-ray diffraction (PXRD). Figs. S10 and 11 (Supporting information) illustrate that the obtained samples are of sod topology, with all the diffraction patterns match with the simulated ZIF-8 pattern [20]. The enhanced Brag diffraction from (222) and (013) planes could be caused by the interactions between PEG molecules and the nucleus of ZIF-8 during the mineralization process [36,37]. FT-IR spectra of the two samples are shown in Figs. S12 and 13 (Supporting information). The bands correspond to =CH– (3131 cm^{-1}), $-CH_3$ (2880 cm^{-1}), –C=C (1576 cm^{-1}), C–O–C (1100 cm^{-1}), confirming the hybridization characteristic of PEG and ZIF-8 in the obtained crystals [36,37]. The PEG/ZIF composites show minimized gas uptake during N_2 adsorption analysis at 77K. Figs. S14 and 15 (Supporting information) suggest that there is almost no uptake at the low relative pressure (< 0.1). In contrast, pure ZIF-8 particles typically can adsorb great amount of N_2 at the low relative pressure region, which is due to the high microporosity of the sod topology. The specific surface areas of the two samples are calculated to be around 50 m^2/g according to the BET theory. The BET surface areas are much lower than that of the pure ZIF-8 crystals (1000 m^2/g). The probable reason is the incorporated PEG molecules can block the pores, rejecting adsorption of N_2 gas molecules. Therefore, bioentities such as sensitive proteins can be packed and protected in the PEG/ZIF composites [36,37].

We take advantage of this synthesizer to fabricate vaccine particles which are ZIF-8 crystals embedded with OVA and CpG (Fig. 4a). The vaccine particles have antigen and adjuvants which are protected by the PEG/ZIF-8 shell. Based on the optimized procedure, we could be able to realize automatic synthesis of the vaccine particles through internet [42]. As a test, we set up a synthesizer with remote control end (Fig. 4b). We input our order in another building which is more than 20 km away from the synthesizer (Fig. S16 in Supporting information).

Figs. 4c and d illustrate SEM images of the two kinds of vaccine particles. The OVA@ZIF-8 particles are of an average size about

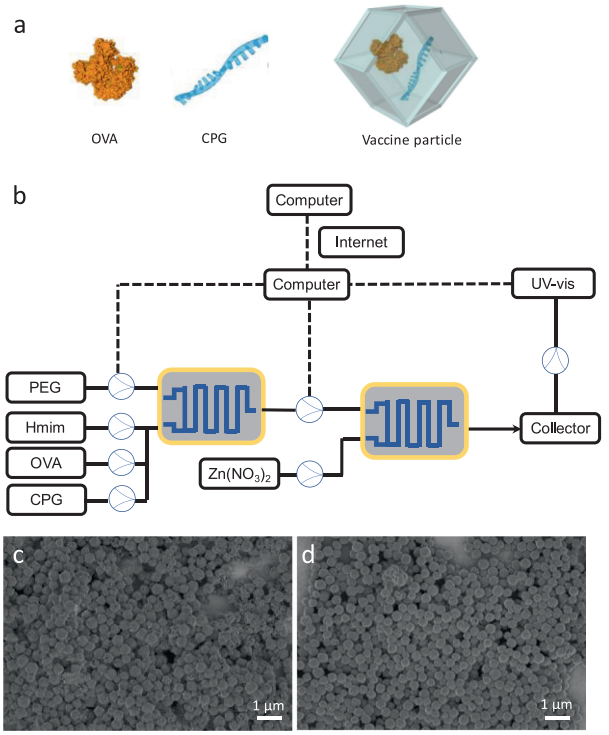

Fig. 4. (a) Illustration of the vaccine particle. (b) Remote automatic synthesis of vaccine particles *via* a flow chemistry synthesizer. (c) SEM image of OVA@ZIF-8 particles. (d) SEM image of OVA-CpG@ZIF-8 particles.

380 nm, while the OVA-CpG@ZIF-8 particles are of an average size about 350 nm. Both samples are smaller than the PEG–only sample (500 nm) by keeping other conditions similar (Fig. 3a). The reason is that the OVA is negatively charged, thus can attract Zn^{2+} ions to the molecules. Nucleation of ZIF-8 can be further accelerated, leading to smaller size of the biocomposite [15]. The PXRD profiles of the two samples match with the simulated ZIF-8 (Figs. S17 and S18 in Supporting information). Only a small additional peak was observed in the OVA-CPG@ZIF-8, indicating the formation of layered ZIF as an impurity (Fig. S18). This is probably due to the influence from the CpG. FT-IR spectra of the two samples confirm incorporation of the OVA and CpG molecules in the ZIF-8 particles (Figs. S19 and 20 in Supporting information). The bands at 3437 cm^{-1}, 617 cm^{-1} and 1250 cm^{-1} correspond to the $-NH_2$ groups of OVA [36,37]. Similar to the PEG-ZIF composite particle, the OVA@ZIF-8 or the OVA@ZIF-8 particles present few uptakes at the low relative pressure (< 0.1) during N_2 adsorption at 77 K (Figs. S21 and 22 in Supporting information) [36,37]. We note that the obtained composites are of similar shape and property like the composites prepared in flask [37]. This is different from the previous report which indicates that the biocomposites prepared in a microfluidic chip contain more defects [32]. The reason is that our microfluidic chips have very good mixing effect, while the reported microfluidic chip intentionally introduce gradient mixing during synthesis [32].

DC activation and maturation is a key prerequisite to generate effective antigen-specific immunity [43,44]. This process is accompanied by increased expression of costimulatory factors and secretion of cytokines [43,44]. To investigate the effects of OVA-CpG@ZIF-8 NPs on the maturation of DCs, the surface markers of the BMDCs were analyzed after cocultivation with different formulations for 24 h. The flow cytometry analysis results showed that the expression of CD86 and CD80 on BMDCs treated by OVA-CpG@ZIF-8 significantly increased than other groups. In contrast, the BMDCs cultured with OVA or CpG showed a slight increase

in expression of costimulatory markers, this may be due to the lack of endocytosis of free antigens and adjuvants (Figs. S23 and S24 in Supporting information). The above results indicate that co-delivery antigen and adjuvant by OVA-CpG@ZIF-8 could efficiently promote DC activation and maturation, triggering robust immune response.

In summary, we presented an automatic synthetic system to prepare PEG mineralized ZIF-8 composite particles. This system is based on flow chemistry with the microfluidic chips fabricated by femtosecond laser micromachining. The sizes of the particles were controlled by the feeding concentration of PEG. The linear relationship between the PEG concentration and the particle size helped to establish an algorithm to synthesize PEG/ZIF-8 composite particles on demand. By combining the addition of OVA and CpG, vaccine particles were synthesized in a modified synthesizer. The vaccine particles can efficiently prompt DC activation and maturation. Furthermore, this synthesizer could be controlled remotely through internet, offering opportunity for future personalized therapy and distributed manufacturing. For instance, the patients may send their special requests to the pharmaceutic company. The automatic factory can manufacture the medicines after receiving the request. We believe the automatic synthetic strategy can be easily integrated with the advanced artificial intelligence technique such as machine learning which can not only save labor work on the bench but also guide unknown synthesis of MOFs or their hybrids.

Declaration of competing interest

The authors declare that they have no known competing financial interests or personal relationships that could have appeared to influence the work reported in this paper.

Acknowledgments

The work is supported by National Natural Science Foundation of China (No. 11674340), Key Project of the Shanghai Science and Technology Committee (No. 18DZ1112700).

Supplementary materials

Supplementary material associated with this article can be found, in the online version, at doi:10.1016/j.cclet.2021.07.004.

References

[1] S. Kitagawa, R. Kitaura, S. Noro, Angew. Chem. Int. Ed. 43 (2004) 2334–2375.
[2] H.C. Zhou, J.R. Long, O.M. Yaghi, Chem. Rev. 112 (2012) 673–674.
[3] Q.L. Zhu, Q. Xu, Chem. Soc. Rev. 43 (2014) 5468–5512.
[4] J.D. Xiao, H.L. Jiang, Acc. Chem. Res. 52 (2019) 356–366.
[5] C.F. Wang, W. Zhang, W.W. Li, et al., Chin. Chem. Lett. 30 (2019) 1390–1392.
[6] C. Chen, D.K. Xiong, M.L. Gu, et al., ACS Appl. Mater. Interf. 12 (2020) 35365–35374.
[7] S.H. Zhang, W. Xia, Q. Yang, et al., Chem. Engin. J. 396 (2020) 125154.
[8] C. Young, J. Kim, Y.V. Kaneti, Y. Yamauchi, ACS Appl. Energy Mater. 1 (2018) 2007–2015.
[9] M. Jin, S.Y. Lu, X.J. Zhong, et al., ACS Sustainable Chem. Engin. 8 (2020) 1933–1942.
[10] J.J. Li, W. Xia, J. Tang, et al., Nanoscale Horizon. 4 (2019) 1006–1013.
[11] J. Liang, X.H. Li, R.B. Xi, et al., ACS Mater. Lett. 2 (2020) 220–226.
[12] J.Y. Cheng, J. Liang, L.B. Dong, et al., RSC Adv. 8 (2018) 40813–40822.
[13] M.D.J. Velasquez-Hernandez, M. Linares-Moreau, E. Astria, et al., Coord. Chem. Rev. 429 (2021) 213651.
[14] X. Fu, G. Zhang, Zhang Y, et al., Chin. Chem. Lett. 32 (2021) 1559–1562.
[15] W.B. Liang, P. Wied, F. Carraro, et al., Chem. Rev. 121 (2021) 1077–1129.
[16] W. Liang, H. Xu, F. Carraro, et al., J. Am. Chem. Soc. 141 (2019) 2348–2355.
[17] C. Yang, J. Xu, D.D. Yang, et al., Chin. Chem. Lett. 29 (2018) 1421–1424.
[18] K. Liang, R. Ricco, C.M. Doherty, et al., Nat. Commun. 6 (2015) 8.
[19] C. Hu, Y.X. Bai, M. Hou, et al., Sci. Adv. 6 (2020) 8.
[20] F. Carraro, J.D. Williams, M. Linares-Moreau, et al., Angew. Chem. Int. Ed. 59 (2020) 8123–8127.
[21] S. Steiner, J. Wolf, S. Glatzel, et al., Science 363 (2019) 144.
[22] A.C. Bedard, A. Adamo, K.C. Aroh, et al., Science 361 (2018) 1220.
[23] C. Empel, R.M. Koenigs, Angew. Chem. Int. Ed. 58 (2019) 17114–17116.
[24] N. Hartrampf, A. Saebi, M. Poskus, et al., Science 368 (2020) 980.
[25] P.J. Kitson, G. Marie, J.P. Francoia, et al., Science 359 (2018) 314–319.
[26] A.J. Mijalis, D.A. Thoma, M.D. Simon, et al., Nat. Chem. Biol. 13 (2017) 464.
[27] D. Perera, J.W. Tucker, S. Brahmbhatt, et al., Science 359 (2018) 429–434.
[28] S.Q. Gao, L. Han, D. Luo, et al., BMC Bioinformatics 22 (2021), doi:10.1186/s12859-020-03915-6.
[29] V. Duros, J. Grizou, W.M. Xuan, et al., Angew. Chem. Int. Ed. 56 (2017) 10815–10820.
[30] R.W. Epps, M.S. Bowen, A.A. Volk, et al., Adv. Mater. 32 (2020) 2001626.
[31] J.G. Li, J.Z. Li, R.L. Liu, et al., Nat. Commun. 11 (2020) 2046.
[32] B.P. MacLeod, F.G.L. Parlane, T.D. Morrissey, et al., Sci. Adv. 6 (2020) eaaz8867.
[33] S. Masubuchi, M. Morimoto, S. Morikawa, et al., Nat. Commun. 9 (2018) 1413.
[34] P. Nikolaev, D. Hooper, F. Webber, et al., NPJ Computational Mater. 2 (2016) 16031.
[35] R. Shimizu, S. Kobayashi, Y. Watanabe, Y. Ando, T. Hitosugi, APL Mater. 8 (2020) 111110.
[36] Q. Yu, Y. Tian, M. Li, et al., Chem. Commun. 56 (2020) 11078–11081.
[37] G. Zhang, X. Fu, H. Sun, et al., ACS Appl. Mater. Interf. 13 (2021) 13978–13989.
[38] W. Li, W. Chu, D. Yin, et al., Appl. Phys. A 126 (2020) 816.
[39] C. Hnatovsky, R.S. Taylor, E. Simova, et al., Appl. Phys. A 84 (2006) 47–61.
[40] Y. Bellouard, A. Said, M. Dugan, P. Bado, Optics Express 12 (2004) 2120–2129.
[41] L.H. Wee, N. Janssens, S.P. Sree, et al., Nanoscale (6) (2014) 2056–2060.
[42] D.E. Fitzpatrick, T. Maujean, A.C. Evans, S.V. Ley, Angew. Chem. Int. Ed. 57 (2018) 15128–15132.
[43] J. Xu, J. Lv, Q. Zhuang, et al., Nat. Nano 15 (2020) 1043–1092.
[44] M.E. Aikins, C. Xu, J.J. Moon, Acc. Chem. Res. 53 (2020) 2094–2105.